Volume 1 | Number 1 | Jan 2013 | Pages 1–100

PCCP

Physical Chemistry Chemical Physics
www.rsc.org/pccp

ROYAL SOCIETY OF CHEMISTRY

ROYAL SOCIETY OF CHEMISTRY

www.rsc.org/pccp

Influence of exothermic chemical reactions on laser-induced shock waves

Jennifer L. Gottfried[a]

RDRL-WML-B,U.S. Army Research Laboratory, Aberdeen Proving Ground, Maryland, 21009, USA

Differences in the excitation of non-energetic and energetic residues with a 900 mJ, 6 ns laser pulse (1064 nm) have been investigated. Emission from the laser-induced plasma of energetic materials (e.g. triaminotrinitrobenzen [TATB], cyclotrimethylene trinitramine [RDX], and hexanitrohexaazaisowurtzitane [CL-20]) is significantly reduced compared to non-energetic materials (e.g. sugar, melamine, and L-glutamine). Expansion of the resulting laser-induced shock wave into the air above the sample surface was imaged on a microsecond timescale with a high-speed camera recording multiple frames from each laser shot; the excitation of energetic materials produces larger heat-affected zones in the surrounding atmosphere (facilitating deflagration of particles ejected from the sample surface), results in the formation of additional shock fronts, and generates faster external shock front velocities (>750 m/s) compared to non-energetic materials (550-600 m/s). Non-explosive materials that undergo exothermic chemical reactions in air at high temperatures such as ammonium nitrate and magnesium sulfate produce shock velocities which exceed those of the inert materials but are less than those generated by the exothermic reactions of explosive materials (650-700 m/s). The most powerful explosives produced the highest shock velocities. A comparison to several existing shock models demonstrated that no single model describes the shock propagation for both non-energetic and energetic materials. The influence of the exothermic chemical reactions initiated by the pulsed laser on the velocity of the laser-induced shock waves has thus been demonstrated for the first time.

Keywords: plasma chemistry, laser-induced shock waves, explosive characterization, laser ablation

I. INTRODUCTION

The interaction of focused laser pulses with different materials has been an active area of study since the invention of the first laser in 1962.[1] Laser ablation has been used for spectroscopic material characterization, sample introduction for chemical analysis techniques, laser machining, laser cleaning, thin film deposition, nanoparticle production, medical applications, etc. The processes involved in the excitation of a material using a high-energy focused laser pulse, including material ablation, expansion into a background gas, plasma ignition, chemical reactions (during and after plasma formation), shock waves, and particle formation are extremely complicated and cannot be described by a single model. The behavior of the excited material is highly dependent on the material properties (e.g., density, thermal conductivity, absorption coefficient, melting point, ionization potential, etc.), the laser properties (e.g., pulse wavelength, duration and energy), and the background gas (e.g., composition and pressure).

---
[a] Electronic mail: jennifer.l.gottfried.civ@mail.mil.

The focus of the current study is how the laser-induced shock wave is affected by the target material properties, especially explosives and other materials that undergo exothermic reactions with air. Most previous studies on laser-induced shock waves used silicon or metal targets and focused on how the shock structure was influenced by the parameters such as the background gas or the laser parameters.[2-15] However, a few studies found that a laser ablated energetic polymer (glyzidyl azide polymer [GAP]) produced a faster shock wave than non-energetic polymers.[16-19] The increased shock wave velocity was attributed to the higher decomposition enthalpy of GAP; the pulsed laser initiated a self-sustaining exothermic reaction resulting in rapid formation of gaseous products. More recently, Roy et al.[20] measured spatially and temporally resolved temperatures behind an expanding laser-induced shock wave to demonstrate differences in energy release between reacting aluminum nanoparticle formulations.Our previous work on laser-induced plasmas generated from energetic material residues explored the chemical reactions that occur during the plasma lifetime.[21-24] Here, the shock wave velocity in the air above the sample surface generated from a large variety of inert and energetic materials was measured in order to determine the effect of exothermic chemical reactions on the laser-induced shock wave. Differences in the laser-induced shock waves resulting from laser-induced plasmas of energetic and non-energetic materials were explored and compared to previous studies.

II. BACKGROUND AND THEORY

During the initial laser-solid interaction, target heating, melting, and vaporization occur. These thermal processes are described by models based on the thermal heat conduction equation.[25] As the material is removed by the pulsed laser, pressure is built up by the volumetric gain of the ablated particles due to the change in their specific volume during the transition from a condensed state to the vapor state. At sufficient laser pulse energies (irradiances $>10^{10}$ W/cm^2), explosive boiling of the target material beneath the surface layer, called phase explosion, leads to mass removal via the ejection of large particles from the sample surface; the ejection of particles can continue for hundreds of milliseconds.[26] Expansion of the evaporated material into the background gas is extremely rapid and can be described by the Euler equations of hydrodynamics.[6,25] Generation of a laser-induced plasma begins by absorption of the laser energy through inverse *bremsstrahlung* processes (absorption of a photon by a free electron), leading to a rapid temperature rise. The hot vapor layer above the sample surface is completely ionized at a pressure substantially above the ambient pressure. Atoms, molecules and ions undergo collisions in a region above the sample surface called the Knudsen layer.[27] Light emission collected from the plasma can thus produce information about the elemental content of the sample in technique called laser-induced breakdown spectroscopy, or LIBS.[28] The LIBS signatures of energetic materials have been extensively investigated for standoff detection applications.[21,29-31] Typical plasma temperatures reach tens of thousands of Kelvin, and are substantially higher for energetic samples than for non-energetic materials.[22]

For longer-pulse lasers (>100 ps), the laser beam is partially absorbed by the plasma through inverse *bremsstrahlung* in a process called plasma shielding.[32] This process can rapidly increase the plasma size and temperature, and is strongly dependent on laser wavelength and pulse duration. Near-infrared laser wavelengths (e.g., 1064 nm) are particularly efficient at heating the plasma compared to visible and ultraviolet wavelengths. Once the laser heating has ended, the plasma begins cooling rapidly for the first 100 ns; after 100 ns, plasma cooling is slowed as energy is regained through recombination and combustion reactions.[22,23] Thermal energy from the material in the plasma is converted to kinetic energy, resulting in high expansion velocities. The expansion of the high pressure vapor acts as a piston driving into the surrounding atmosphere, compressing the ambient gas at its front into a thin shell. For laser ablation, the force of this piston depends on the volume of gas produced, which is related to both the ablated mass and to the temperature reached in the plasma plume. Energy is

transferred to the surrounding air through a combination of thermal conduction, radiative transfer, and heating by the resulting shock wave. At high laser irradiances, shock heating dominates.[33]

When the plasma dynamics are determined by absorption of the laser radiation within the plasma, the shock wave is similar to a detonation phenomenon and is called a blast wave.[3,34,35] Both the laser-induced plasma generated from a thin film of material applied to a glass substrate and the shock structure of the resulting blast wave are shown in figure 1. The arrows indicate the direction of propagation for the plasma and various fronts. The presence of the contact fronts, ionization front, and shock front have been confirmed through shadowgraph imaging, e.g., Callies et al.[4] The propagation of the blast wave is determined by the amount of energy released into the plasma state and can be described by the Sedov-Taylor theory.[3,4,36] For spherical propagation, the relationship between the distance travelled by the blast wave R and the energy converted into the plasma state ΔE is given by

$$R = \lambda \left(\frac{\Delta E}{\rho_0}\right)^{1/5} t^{2/5}, \tag{1}$$

where λ (with an approximate value of 1) is a dimensionless quantity depending on the gas-dynamical state of the air, ρ_0 is the mass density of the undisturbed air and t is the time of propagation (assuming the laser pulse duration $< t$ and the laser spot diameter $< R$). Equation (1) is only valid when the mass of the energy source is negligible compared to the mass of the surrounding air that is swept up by the expanding shock (i.e., not valid at very early times) and when the pressure driving the shock front is much larger than the pressure ahead of it ($R \ll (\Delta E/\rho_0)^{1/3}$), a condition not met after a certain distance. The expansion of the shock wave produced with a nanosecond laser was found to be spherical and proportional to $t^{2/5}$ from about 3-100 ns.[5]
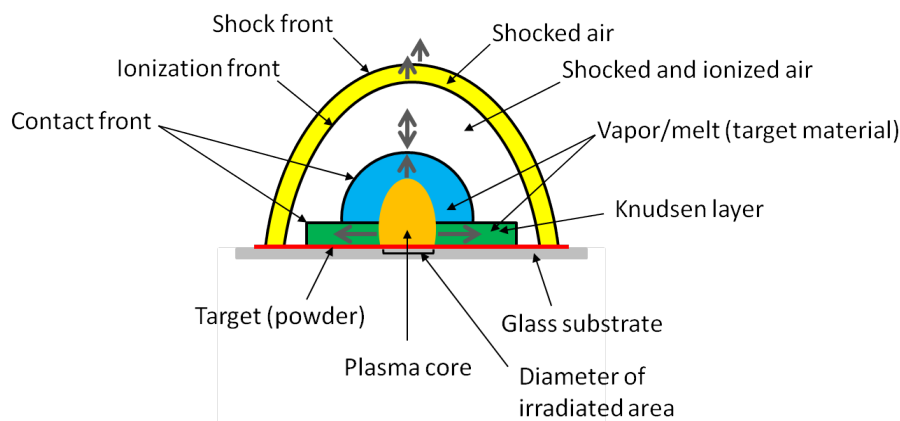
FIG. 1. Laser-induced plasma and shock structure (adapted from Callies et al.[4]).

At high laser irradiances (typically greater than 10^7 W/cm^2), a shock front analogous to a detonation wave can be ignited from nearly any material.[37] The interaction of the laser beam with the plasma results in compression of the vaporized gas by the absorption of the laser energy, contributing to the heating and ionization of the ablated material. The velocity in this region is supersonic with respect to the ambient gas and a shock wave known as a laser-supported detonation wave (LSDW) is produced.[26,37-41] The name LSDW originated from its similarity to a chemical explosion, which propagates by shock compression of a combustible mixture. In this regime, laser energy is absorbed by the plasma in front of the shock wave and the shock wave is efficiently enhanced; at irradiances lower than 10^6 W/cm^2 laser-supported combustion occurs and the laser

energy is absorbed in the plasma behind the shock wave with no contribution to the thrust from the blast wave expansion.[41] The properties of the LSDW are dependent on the gas species and the pressure through which the wave propagates. The LSDW creates a high temperature and pressure region that enables atomic and molecular reactions that could lead to a chemical detonation. For example, Kim et al.[42] compared the initiation of chemical reactions between ablated aluminum and oxygen from the air with a high-power laser pulse to the classical detonation of exploding aluminum dust in air, while Gottfried[22] investigated the chemical reactions between laser-ablated metal particles and the explosive cyclotrimethylenetrinitramine (RDX). Typical shock wave velocities near the laser-material interaction region are tens of km/s, corresponding to pressures of tens or hundreds of GPa.[6,26] Unlike the spherical blast wave which propagates normal to the sample surface, the LSDW is conical in shape and propagates along the direction of the laser beam (figure 2). The LSDW lasts only as long as the propagation conditions are satisfied during the laser pulse, i.e., as the laser beam diverges with increasing distance from the target the wave degenerates into an combustion wave with a much smaller absorption coefficient.
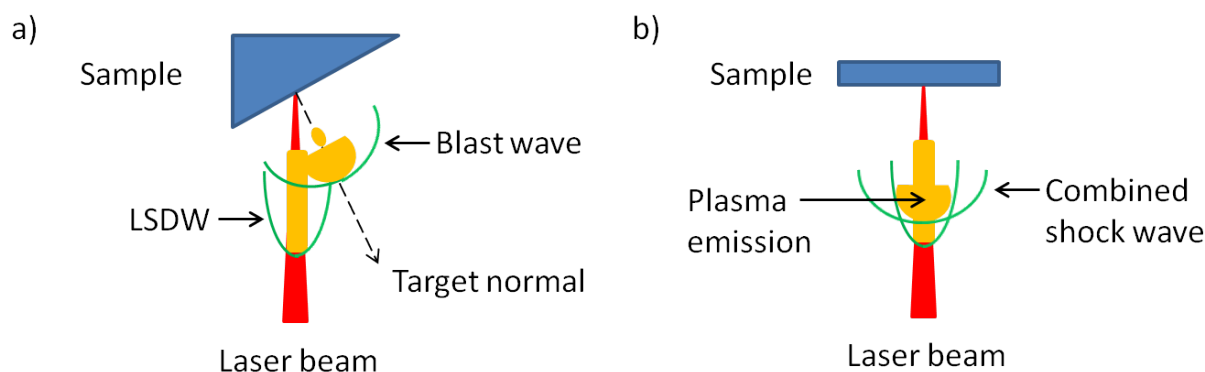
FIG. 2. Comparison between the LSDW and the blast wave, which are distinct when the laser interrogates the sample off-angle (a) and combined when the propagation of the laser is perpendicular to the sample (b).

As the shock wave expands into the ambient atmosphere, resistance from collisions of the shocked air with the background gas decelerates the shock wave; an internal shock wave generated by the deceleration of the contact front by the background gas is propagated back towards the target surface and is reflected back and forth between the sample surface and the external shock front until the external shock has dissipated into a sound wave. At these later times the distance of the external shock wave from the target R can be described by a drag model,[43] which is given by

$$R = R_0\left[1 - e^{-\beta t}\right], \tag{2}$$

where R_0 is the stopping distance of the shock wave and β is the slowing coefficient (resulting from resistance caused by collisions with the background gas). Eventually the shock is dissipated as a result of this drag/resistive force. Previous studies on the expansion dynamics of the laser-induced plasma have shown that the plume expansion follows the blast wave model (equation 1) up to 300 ns[44] and the drag model is a good approximation of the plume front velocity $v_0 = R_0\beta$ from 500 to 2000 ns.[27] At times greater than 4 μs, the drag model was found to predict distances slightly shorter than those observed experimentally.[45] Similar results have been obtained for the shock wave expansion, although most papers use either equation (1) or equation (2) depending on the experimental conditions.[4,5,8,10-13,15,20,43,46-51] Following the laser-induced plasma and

subsequent shock wave formation, ejected material above the sample surface can begin to deflagrate several milliseconds after the initial laser shot (especially for energetic materials); this deflagration can last for hundreds of milliseconds.

III. EXPERIMENTAL

Energetic material samples were obtained from colleagues at the U.S. Army Research Laboratory (ARL); materials investigated included black powder, smokeless gun powder, 1,3-dinitrobenzene (m-DNB), 1,4-dinitrobenezene (p-DNB), 2,4-dinitroanisole (DNAN), trinitrotoluene (TNT), RDX (Class 1 and Class 5), hexanitrostilbene (HNS), triaminotrinitrobenzene (TATB), 3-nitro-l,2,4-triazole-5-one (NTO), pentaerythritol trinitrate (PETN), cyclotetramethylene tetranitramine (HMX), hexanitrohexaazaisowurtzitane (CL-20), composition-A3 (RDX with 9% oxidized polyethylene), composition-B (60% RDX, 40% TNT), and pentolite (50% PETN, 50% TNT). Non-explosive materials including ammonium nitrate (AN)(NH_4NO_3), Epsom salt ($MgSO_4 \cdot 7H_2O$), L-glutamine ($C_5H_{10}N_2O_3$), melamine ($C_3H_6N_6$), sugar (sucrose, $C_{12}H_{22}O_{11}$), graphite nanoparticles (GNP; 3-4 nm), nanographite (NG; 1-4 μm wide, 50 nm thick), diamond grit (25-35 μm), and graphite lubricant (micron-sized particles) were obtained from various commercial sources. All samples were prepared on the same substrate – double-sided tape affixed to a glass micro slide (25×75 mm). Approximately 10-20 mg of each material was applied to the tape surface and distributed across the surface with a spatula. Excess material was removed by gently tapping the slide. Since the shock wave from each laser shot removed material from a diameter approximately 500% larger than the diameter of the focused laser, subsequent laser shots were spaced to avoid disturbed areas of the sample surface. A total of 5-8 laser shots were obtained from each sample slide.

The laser pulse from a Nd:YAG laser (Quantel Brilliant b) was focused on the sample surface with a 10 cm lens (Table I). In order to prevent breakdown of the air above the target, the plane of the target surface was placed 1.5 mm above the focal point of the lens (i.e., 1.5 mm closer to the lens). The estimated diameter of the focused laser beam based on the average crater size on several metal targets was 0.8 mm. The highest laser pulse energy attainable with this laser was used in order to ensure breakdown of any target material and to ensure formation of a LSDW. Because the energetic materials were applied in a thin layer and shocked with a nanosecond-pulsed laser that is not sufficient to initiate the secondary energetic materials, no detonation wave was generated through the bulk energetic material. A strong exhaust inlet was positioned next to the sample stage to remove vapors and particulate matter. The influence of the exhaust on the ablated material was not observed until several milliseconds after the initial laser pulse, when the heated air, unreacted particles, and deflagrating particles (for energetic materials) were pulled towards the exhaust (to the left of the camera view).

TABLE I. Parameters for the Nd:YAG ablation laser.

Laser parameter	Value
Pulse wavelength λ	1064 nm
Pulse duration t_p	6 ns
Maximum pulse energy E_p	900 mJ
Spot Area A	5.0×10^{-3} cm^2
Fluence ε	180 J cm^{-2}
Peak power density (irradiance) I	3.0×10^{10} W cm^{-2}

The schlieren imaging technique[52] was used to visualize the laser-induced shock wave in air. Figure 3 shows a simplified schematic of the experimental setup. An arc lamp (Newport Oriel model 66476) with a 200 W Hg-Xe ozone-free lamp

(model 6290) served as the illumination source, which was focused onto the 1st mirror with an aspheric condenser lens. The light was collimated between the two schlieren mirrors (10.8 cm diameter, 114 cm focal length), which were spaced 211 cm apart. The sample was placed on a vertical stage in the test section between the two mirrors, and the ablation laser was focused on the sample surface from above. Changes in the refractive index of the air caused by the formation of the laser-induced plasma bent the light rays, so that when the light was focused after the 2nd mirror, a knife edge placed at the focal spot could be used to cut out approximately half the light rays; the schlieren images thus correspond to the first spatial derivative of the index of refraction. A high-speed color camera (Photron SA5) was used to record the light and dark striations in the images representing differences in the refractive index of air in the test region. A zoom lens (Nikon Nikkor 24-85mm f/2.8-4D IF) on the camera was focused 33 cm in front of the focus of the ablation laser. This focal position was optimized to provide the greatest contrast for visualization of the shock wave. The following camera settings were used for imaging the shock waves: 84,000 frames per second (fps), 1.0 μs shutter, 64×648 pixels image size. A custom program written in Matlab (R2013a) was used to scale the images and measure the shock position at each camera frame.
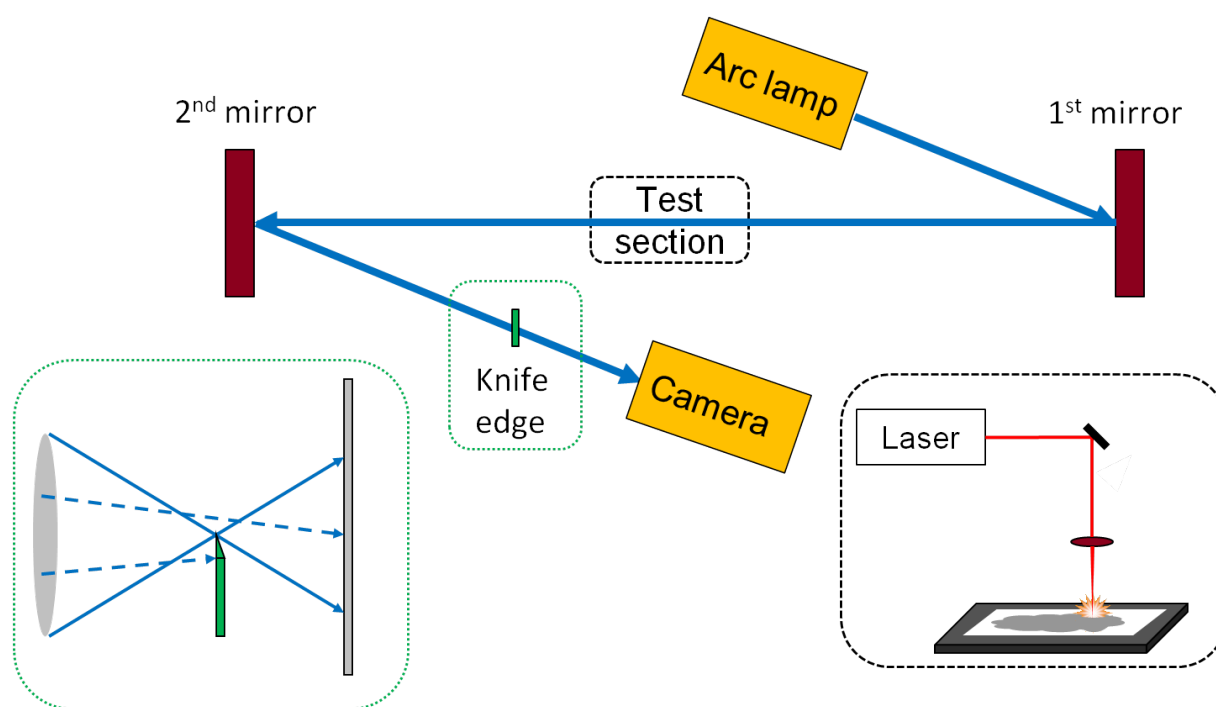
FIG. 3. Experimental setup for schlieren imaging of the laser-induced shock wave. The laser-induced plasma is generated in the test section between the 10.8 cm diameter mirrors (114 cm focal length); differences in the refractive index of air observed in the test section are observed by using a knife edge to cut-off approximately half of the light rays imaged by the high-speed camera.

IV. RESULTS AND DISCUSSION

A. Evidence for LSDW

LSDWs propagating towards the laser source have been observed in the shadowgraph images of laser ablated brass targets in air[11] and aluminum targets in both air[42] and argon.[13] Since at a maximum the LSDW lasts only as long as the laser pulse (6 ns duration in this experiment) and the distortion of the external shock front by the LSDW (caused by non-uniform heating of

the central tip of the vapor plume) lasts less than 300 ns, direct observation of the LSDW was not possible with the current experimental setup; however, indirect evidence for the LSDW has been observed. Figure 4 shows several snapshots from the high-speed schlieren video (12,000 fps; 9.8 μs shutter) of the laser-ablated blank tape substrate. In the first frame, the shock wave (**A**) and plasma plume (**C**) were observed. In addition, a thin column of heated air (**B**) above the plasma plume was observed. This region is evidence for the presence of a LSDW during the laser pulse. As the plasma cools and the atomized and excited carbon combusts in the air (at times greater than 83 μs), the density gradient caused by the high-temperature plasma is no longer distinguishable from this region.
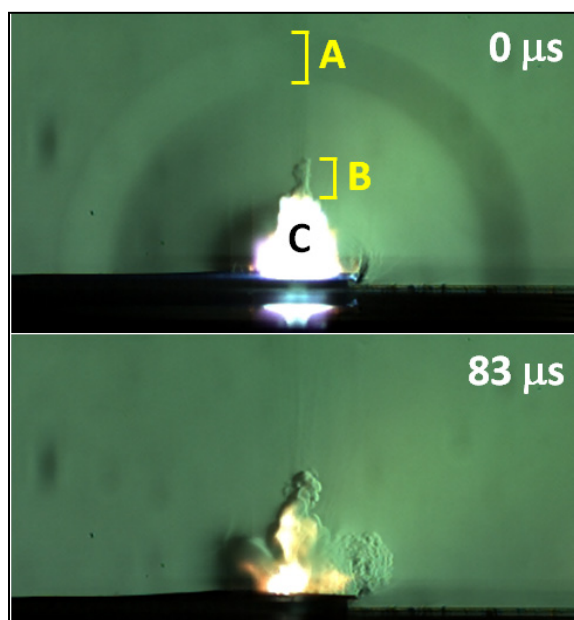
FIG.4. Snapshots from the laser-ablation of the blank tape substrate showing the shock front (A), the density gradient providing evidence for a LSDW (B), and the plasma volume (C).

Under some conditions, a faster moving component of an expanding plume front can split into two clouds (plume splitting).[27] High-speed speed video of a black plastic substrate (figure 5) was obtained with the laser normal to the substrate (**a**) and with the sample on a 30° incline (**b**). When the laser was perpendicular to the substrate, plume-splitting was observed, while no plume-splitting occurred with the sample on an incline. We postulate that the additional energy from the LSDW in the direction of the laser beam (coinciding with the propagation direction of the blast wave) resulted in the observed plume-splitting (figure 5**a**). In combination with the relatively high laser fluence (table I) and heated region of air surrounding the location of the laser beam (figure 4), this suggests that a LSDW was present at very early times under the current experimental conditions and likely influenced the plasma chemistry and shock formation.
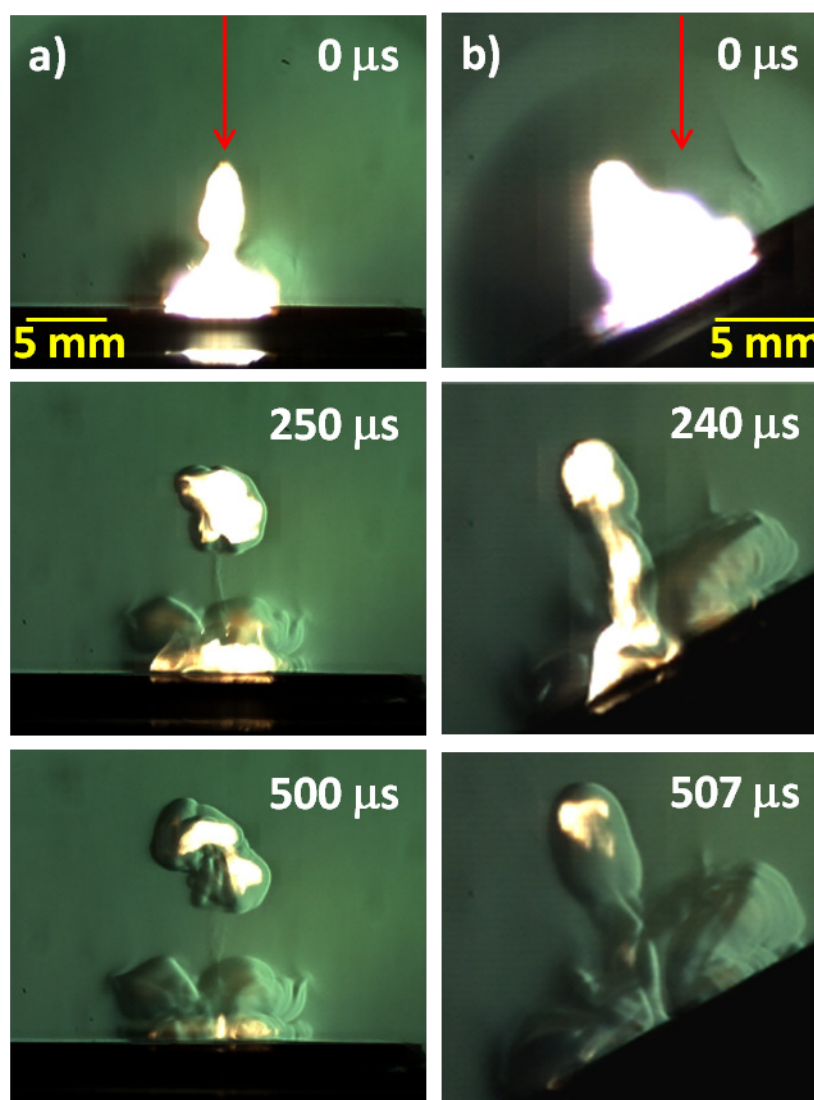
FIG. 5. Evidence for LSDW: a) plume-splitting observed when the laser propagation coincides with blast direction, but not when b) the substrate is on a 30° incline.

B. Laser excitation of residue organic materials

Figure 6 shows snapshots from the schlieren videos (12,000 fps at full camera resolution, 9.8 µs shutter) of the laser ablation of a non-energetic material (L-glutamine) and an energetic material (RDX). The first frame after the laser pulse (0 µs) shows the laser-induced plasma, which is typically more luminescent for non-energetic materials. Because of the decrease in brightness, the laser-induced shock wave is visible in the first frame of the RDX video. The second frame (83 µs) shows the roughly hemi-spherical propagation of the shock wave (which is faster for the RDX). The vertical height of the shock wave was approximately 50% of the horizontal diameter at the target for both samples. The high-resolution video also shows the ejection of material from the target surface resulting from the impact of the internal shock wave. By 500 µs, the light emission was gone for both materials and the heat-affected zone in the background air caused by the plasma formation was clearly visible for both samples; the RDX produces a significantly larger zone. At later times (greater than 1 ms), the pull of the exhaust (to the left of the images) on the heated air and unreacted particles was observed for the L-glutamine. By 15 ms,

8

RDX particles ejected from the sample surface started deflagrating as they reached the heated air above the sample surface (resulting in additional light emission and rapid vertical and horizontal expansion of the heated area).
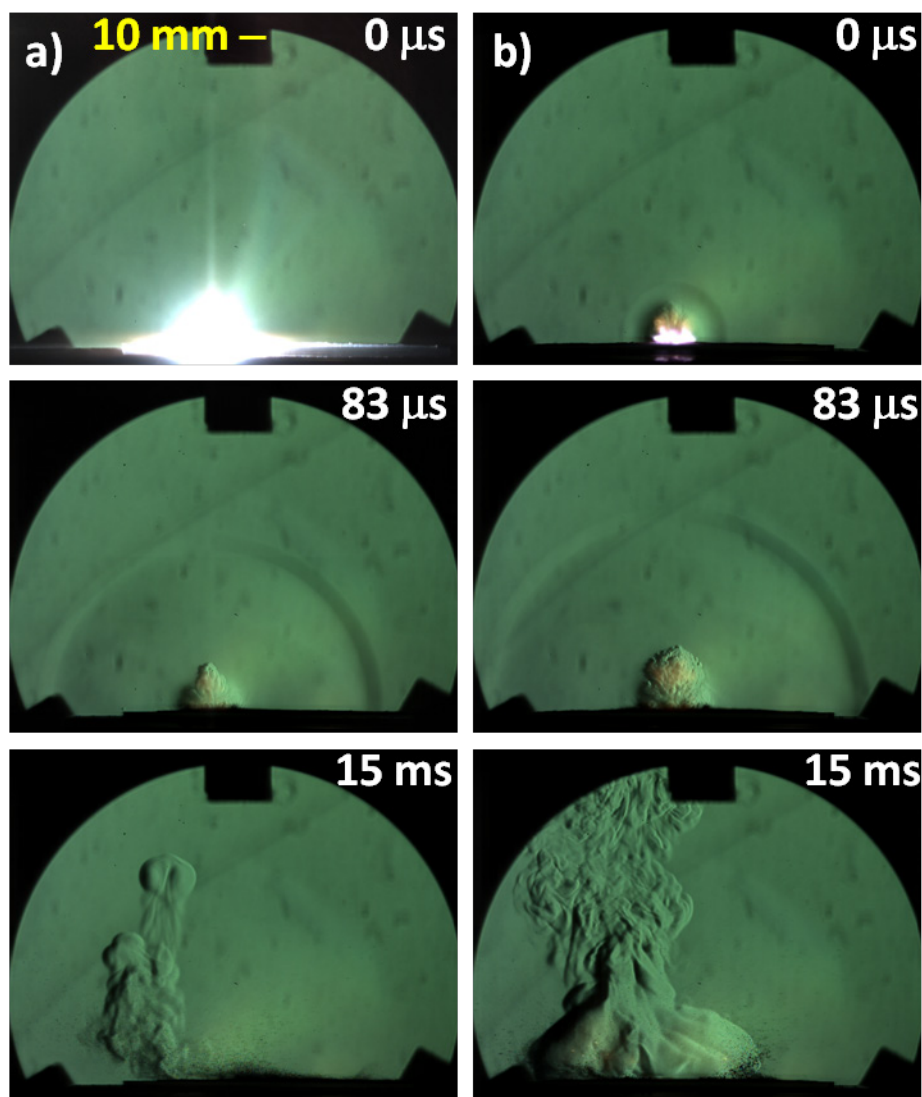
FIG. 6. Schlieren images of laser-shocked a) L-glutamine and b) RDX.

Evidence for phase explosion was also observed in the high-speed video for the laser ablation of the blank tape substrate (not shown). Large pieces of the tape (from 579 to 925 μm) were observed moving away from the sample surface at slower velocities than the shock wave. This effect was only observed for the blank tape. A possible explanation is that the laser pulse passed through the tape (which is transparent to 1064 nm light), where heat was trapped between glass slide (positioned on a black sample stage) and the back of tape, leading to explosive boiling. On the other hand, when a thin layer of energetic (or non-energetic) material is affixed to the tape, most of the laser energy interacts with the material. This interaction, and subsequent interactions between the reflected internal shock wave and the sample surface lead to ejection of the particles from the sample surface. Some of these particles are atomized in the laser-induced plasma. The remaining particles pass through the heated atmosphere, which can lead to combustion or deflagration in air (figure 7). None of the non-energetic

samples deflagrated under these experimental conditions. All the energetic material samples in this study (except for the granular black powder and smokeless gun powder) deflagrated.
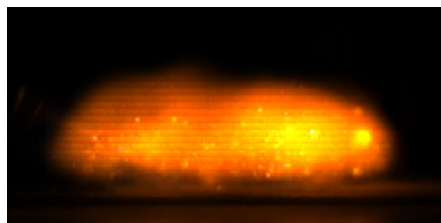
FIG. 7. Snapshot from the direct high-speed video of the laser-induced deflagration of RDX (9 ms after the laser excitation; the width of the deflagration region is 50 mm).

The most obvious difference in the high-speed videos (84,000 fps; 1 μs shutter) of the laser-material interaction between non-energetic (inert) materials and energetic materials is the luminosity of the plasma emission. Inert materials result in an intensely brilliant white light in the first camera frame from continuum emission of the laser-induced plasma (figure 8**a-d**); the resulting shock front is clearly visible in subsequent frames. Plasma lifetimes for most materials last hundreds of microseconds with a 900 mJ focused laser at 1064 nm; when the camera is focused in front of the laser-induced plasma as in figure 8, however, the emission appears significantly more diffuse. Light emission from the secondary high explosives (**e-h**) looks distinctly different. Because of the decreased plasma luminosity, the shock front is observable from the first camera frame.

Epsom salt and AN undergo exothermic chemical reactions in air following laser excitation. Magnesium sulfate is a naturally occurring, hygroscopic inorganic salt used in the manufacturing of explosives and matches. Magnesium sulfate and atomized magnesium atoms will react via the exothermic reaction[53]

$$MgSO_4 + 4\ Mg \rightarrow MgS + 4\ MgO. \tag{3}$$

The green emission visible in the high-speed video (figure 8**i**) of laser-excited Epsom salt is due to the strong emission of Mg I at 517.3 and 518.4 nm[54] (confirmed by wavelength-resolved emission spectra) . AN is a poor explosive by itself because it is overoxidized and extremely difficult to initiate; it is used safely as a fertilizer in multitonnage quantities but is also an effective explosive when mixed with a suitable fuel. Upon heating, AN will decompose according to the exothermic reactions[55]

$$NH_4NO_3 \rightarrow N_2O + 2\ H_2O \tag{4}$$

$$NH_4NO_3 \rightarrow N_2 + 0.5\ O_2 + 2\ H_2O. \tag{5}$$

In the presence of a fuel, the following exothermic reaction occurs

$$2\ NH_4NO_3 + C \rightarrow 2\ N_2 + CO_2 + 4\ H_2O. \tag{6}$$
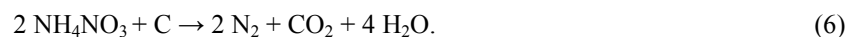
The tape may provide a limited fuel source for the AN reaction. The orange emission visible in the high-speed video (figure 8**j**) is due to the relatively large concentration of Na impurities in the sample (with strong emission at 589.0 and 589.6 nm[54]).
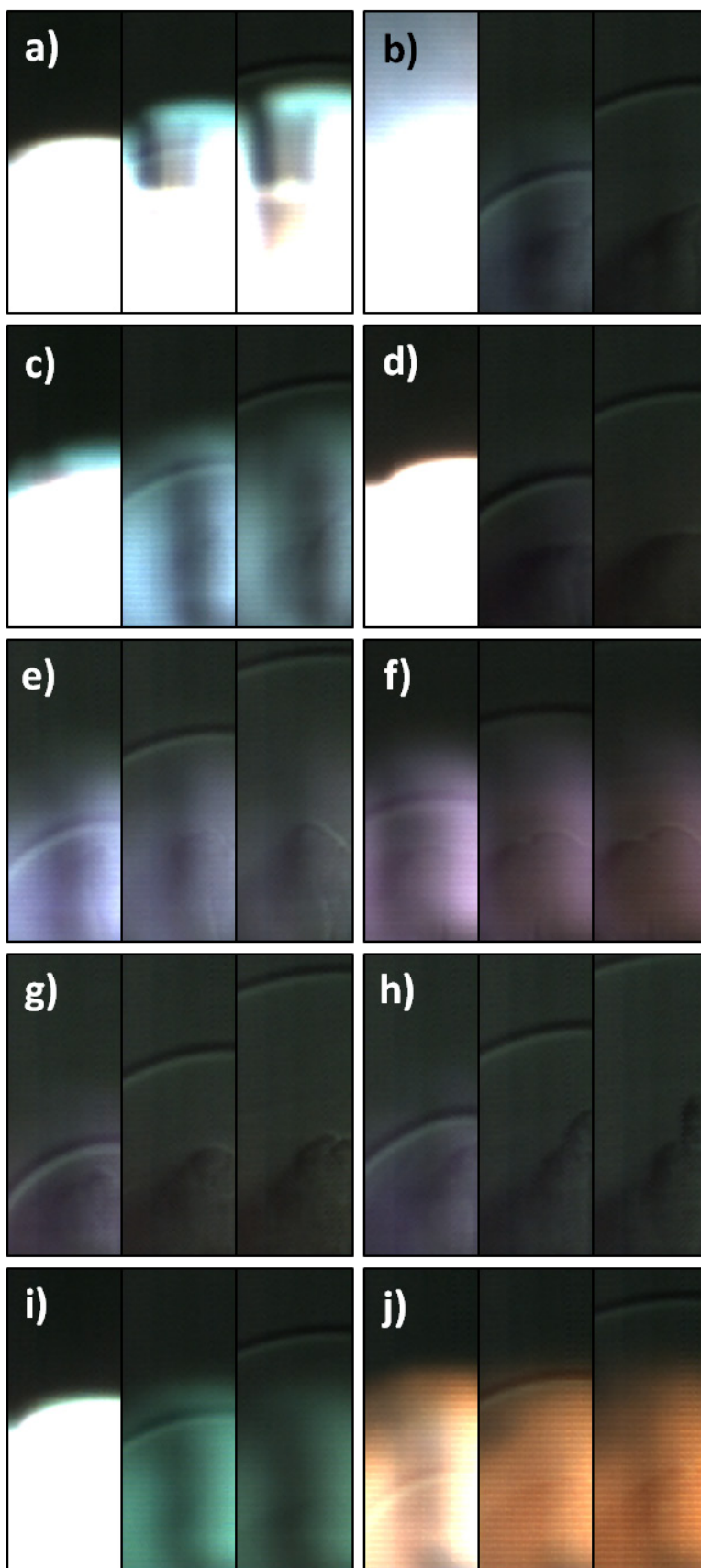
FIG. 8. Light emission from non-energetic phnd energetic materials: a) GNP, b) L-glutamine,c) melamine, d) sugar, e) TNT, f) TATB, g) RDX, h) HMX, i) Epsom salt, and j) ammonium nitrate.

C. Shock front propagation

Multiple shock fronts have been identified in the literature for laser ablated materials. In addition to the LSDW travelling at Mach 3, Maher and Hall[37] observed a second wave travelling near Mach 1 (which they postulated was from the sample material vaporization), and a third wave travelling near Mach 0.5. Callies et al.[4] observed multiple discontinuities, which they attributed to the kinetic energy of the evaporated material accelerating the ambient gas, the contact front between the plasma and the shocked air, the contact front between the evaporated material and the shocked gas, the interface between the target material and the air, and the high temperature plasma region. Wen et al.[7] used femtosecond shadowgraphy to track what they described as an internal shock wave, an external shock wave, a LSDW, and a laser-supported combustion wave. Harilal et al.[13] observed a primary shock followed by a secondary shock that they attributed to the internal shock-wave structure within the plasma plume.

When the outward-moving external shock wave forms, an internal shock wave develops to balance the velocity and high backpressure generated by the external shock wave when the vapor plume expands supersonically; this internal shock wave propagates back towards the target surface. When the internal shock impacts the target surface, it is split into two shocks – one travels through the target material and another propagates back toward the main external shock; when the internal shock wave catches up to the contact surface, it is reflected back toward the target surface again. This reflection-transmission phenomenon can repeat multiple times, generating new refracted external shocks.[6,56] Because the target in this experiment is a thin layer of material affixed to transparent tape on a glass slide, a strong enough internal shock could also transmit through the sample until it hits the sample stage and is reflected back towards the external shock.

Figure 9 shows the first 15 frames from the high-speed video (84,000 fps; 1 μs shutter) from the laser ablation of the blank tape substrate. The initial frame captures the first microsecond of the event – each successive frame is 11.9 μs later; the first 15 frames thus capture the first 178.5 μs (at later times the external shock has travelled outside the field of view of the 10.8 cm schlieren mirrors). In the top part of figure 9, the camera was focused in front of the laser-induced plasma to optimize visualization of the three shock fronts (**1-3**). The dark band is the expanding external shock front, while the light band immediately following the main shock front is a result of refracted light rays. Two additional shock fronts were observed at later times. In the bottom part of figure 9, the camera was focused on the laser-induced plasma so that the expansion of the plume (**4**) and the expansion of the column of heated air from the LSDW (**5**) could be tracked.
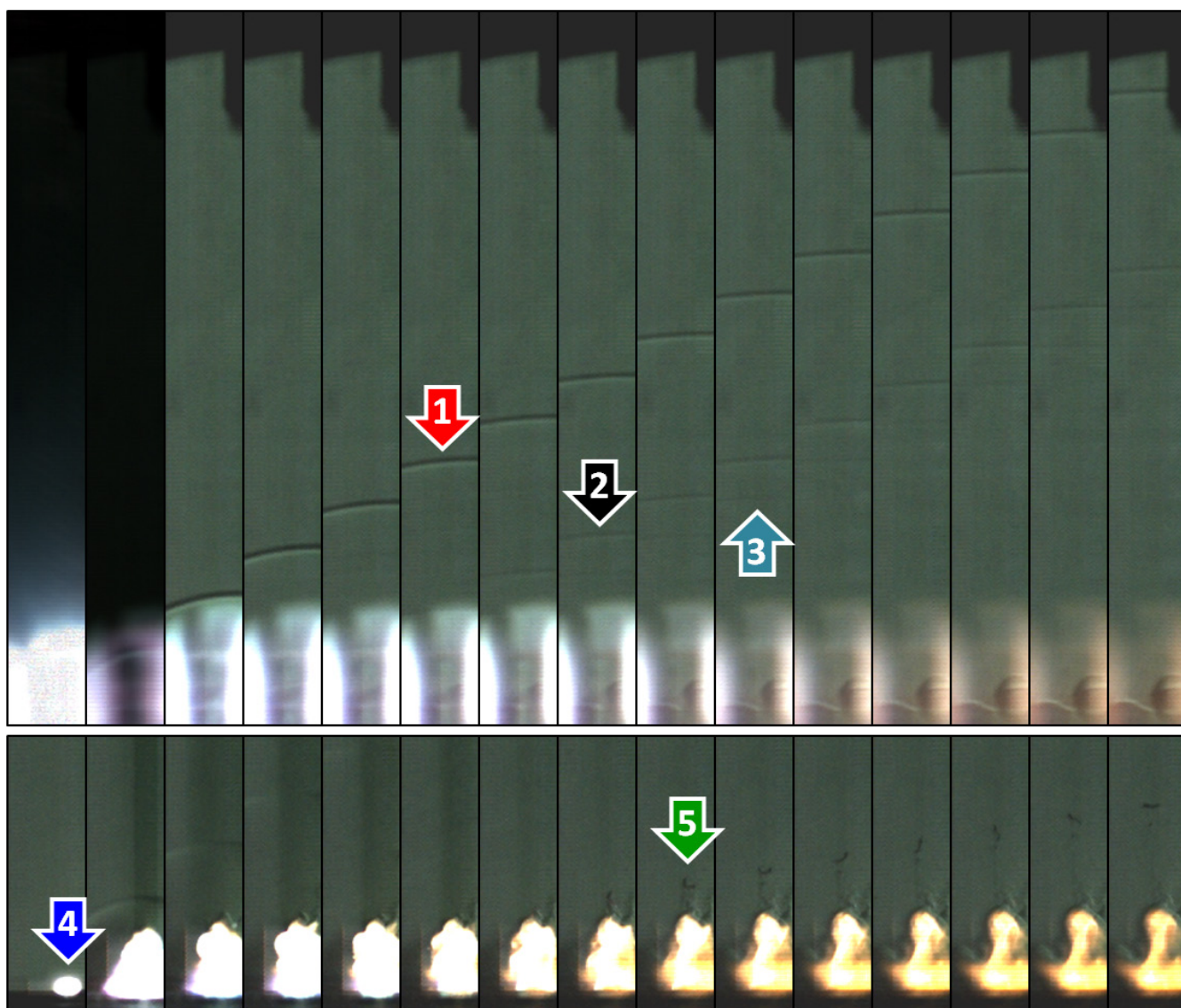
FIG. 9. Blank tape substrate with the camera focus in front of plasma (top, focus 33 cm closer to 2nd mirror) and on the plasma (bottom); 1=primary shock front, 2=2nd shock front, 3=3rd shock front, 4=plasma front, 5=density gradient extending away from target surface towards the laser.

The position-time plot (*R-t*), or timeline, for the plasma plume position, density gradient position, and shock front positions for the non-energetic L-glutamine is shown in figure 10 (top). The main external shock wave was not observed until about 10 mm above the target surface due to the strong plasma emission. After about 60 μs, a second shock front was observed; a third appeared after approximately 70 μs. The region of heated air above the plasma plume was about three times larger (in height) than for the blank tape substrate. The shock timeline for an energetic sample (bottom of figure 10), RDX, looked quite different. The laser-induced plasma was significantly less luminous and all visible emission was gone after 85 μs. The heat-affected zone above the laser-induced plasma was extremely large compared to the blank and L-glutamine. The second and third shock fronts appeared much earlier at 35 μs, and fourth and fifth shock fronts appeared after 60 μs. Unfortunately with this experiment it was not possible to definitely determine the origin of the additional shock fronts, however, their presence is likely indicative of the extra energy released during the laser ablation of an energetic material and the subsequent exothermic reactions in the laser-induced plasma.[22] For example, a strengthened internal shock wave would

undergo more internal reflections and generate stronger refractive shock fronts. The external shock wave velocity was also faster for the energetic material. Although the velocity of the shock wave decreases with each successive frame (approaching the speed of sound in air at 343 m/s), the laser-induced shock wave had not yet decayed into a sound wave by the final camera frame for any of the samples.
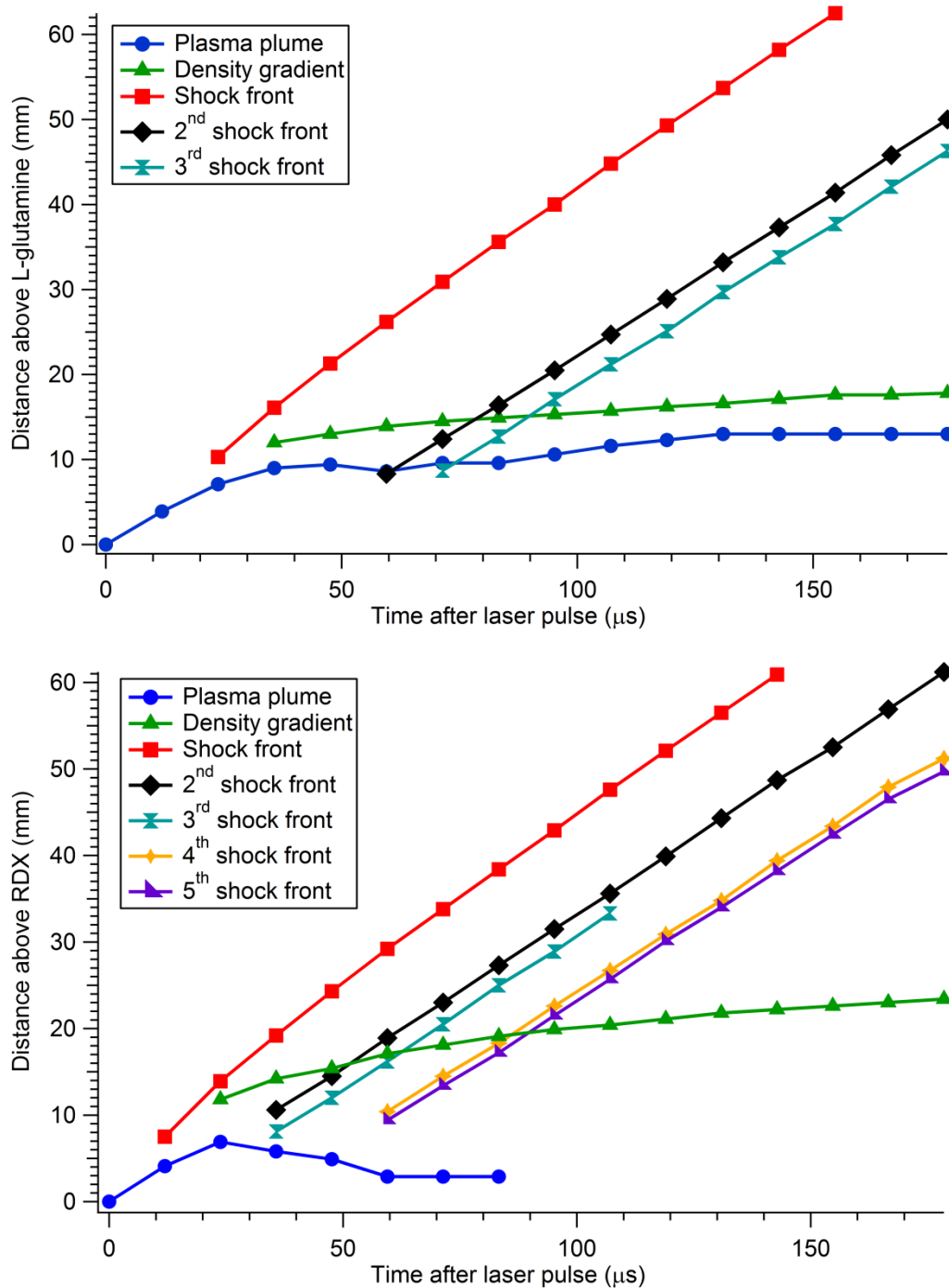
FIG. 10. Shock timelines for L-glutamine (top) and RDX (bottom).

D. Measurement of shock velocities

Typically expansion velocities are determined by the derivative of the position-time graph, where the data is fit to a model based on classical point blast theory. Most papers that measure the laser-induced shock wave apply the Sedov-Taylor relationship (equation 1), which predicts an exponential factor of 0.4. Figure 11 shows the fits for data obtained from both energetic and non-energetic materials to an equation of the form $R=At^q$. The goodness of each fit is indicated by the χ^2 statistic, which is given by

$$\chi^2 = \sum \frac{(y - y_i)^2}{\sigma_i^2} \tag{7}$$

where y is the fitted value for a given point, y_i is the measured data value for the point, and σ_t^2 is an estimate for the standard deviation of y_i. A smaller value of χ^2 indicates a better fit, while a value less than 1 indicates the model is over-fitting the data.
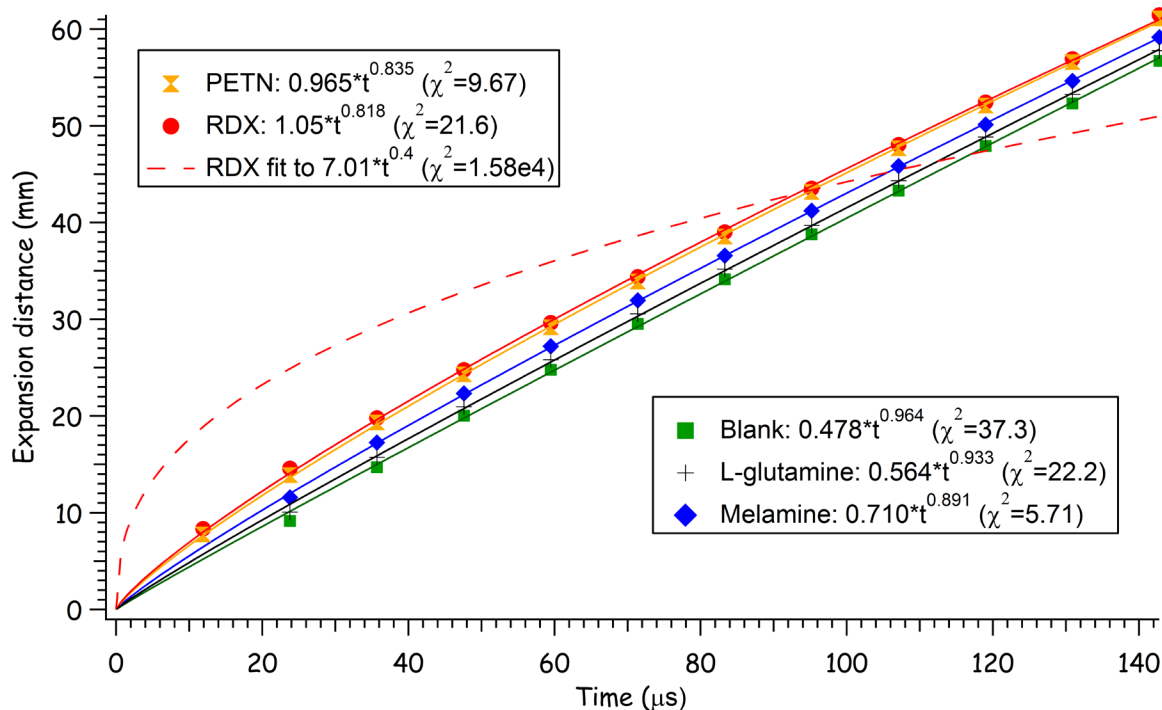
FIG. 11. Expansion distance of the shock waves vs. time demonstrating that the Sedov-Taylor relationship ($\sim t^{0.4}$) is not valid at these distances.

While a power function describes the expansion distance of the shock waves versus time reasonably well, the exponential factor q is much higher than 0.4 (close to 0.9 for the non-energetic materials and 0.8 for the energetic materials). Classical point blast theory assumes energy is instantaneously released into the surrounding atmosphere from an essentially massless point source, forming a spherical shock wave.[34] This neglects the effect of exothermic reactions occurring after the initial laser pulse. In addition, the strength of blast wave must be sufficiently large enough to neglect the ambient gas pressure in comparison with the pressure behind the shock wave, an assumption that is not valid at longer distances when the shock wave begins to decay. The treatment of weak shock waves requires inclusion of source mass[57] or counterpressure,[36]

approximate expressions that need to be solved numerically. Although many previous studies have successfully applied the Sedov-Taylor theory to laser-induced shock waves, most used non-reactive materials and observed the shock wave at shorter timescales (less than 1 μs).

Previous studies have shown that decreasing the atmospheric pressure[27,43,46] or using a laser spot size of the same magnitude as the measured shock wave distance[58-60] can result in higher exponents. In this experiment, the diameter of the focused laser was 0.8 mm and the first image of the shock wave was obtained a minimum of 7 mm above the sample surface. Only a few papers have reported $q>0.4$ at standard pressure. Srinivasan et al.[61] reported an exponent of 0.76 for the shock wave expansion of a laser-ablated organic substrate, polymethylmethacrylate. No explanation for the deviation from Sedov-Taylor theory was given. Schmitz et al.[51] attributed the higher exponents obtained for various organic materials (0.48-0.68) to the relatively low laser fluences (<1.0 J/cm^2) used in their experiment; this explanation would not apply to the current experiment. If the dynamics of the shock front are determined by the volumetric gain of particles caused by the change in their density during the transition from the condensed to the vapor state and the subsequent heating of the plasma resulting from absorption of laser radiation, then the Sedov-Taylor scaling is not applicable.[35] In the current experiment, the presence of the LSDW and the significant plasma shielding that occurs with a 1064 nm pulse at 900 mJ result in significant plasma heating. Based on the high exponential factors ($q>0.4$) observed for both energetic and non-energetic materials, classical point blast theory clearly does not apply under the current experimental conditions.

While classical Sedov-Taylor blast wave theory is only valid when the energy behind the shock wave comes from a point source, variants of the theory have been developed to account for the mass contribution of the point source.[57,62] Following this approach, when the shock wave radius is fit to a power law dependence of the form

$$R(t) = At^\alpha, \tag{8}$$

the time-dependent energy takes the approximate form

$$E(t) = \frac{8\pi\rho_0(3\gamma-1)}{3(\gamma+1)^2(\gamma-1)} A^5 \alpha^2 t^{(5\alpha-2)}, \tag{9}$$

where ρ_0=1.20 kg/m^3 and γ=1.4 for the density and specific heat capacity of the unshocked air, respectively, and A and α are the fitting parameters from equation (8). Using equation (9) and the fits shown in figure 11, the time-dependent energies for the inert and energetic samples are shown in figure 12. This treatment assumes that the contribution of the solid-phase particles is negligible over the observed timescale and that the heat capacities for the laser ablated material and ambient gas are equivalent; the absolute magnitudes of the estimated energy release have previously been shown to be unrealistic,[20] although in that case the calculated energies were significantly higher than the energy put into the system with the ablation laser. The estimated energy values do, however, enable comparison of the relative magnitudes of energy release for each sample. The energy release from the energetic samples is much more significant than for the non-energetic samples at $t>10$ μs; only the energetic samples undergo exothermic combustion reactions leading to eventual deflagration (after several milliseconds).
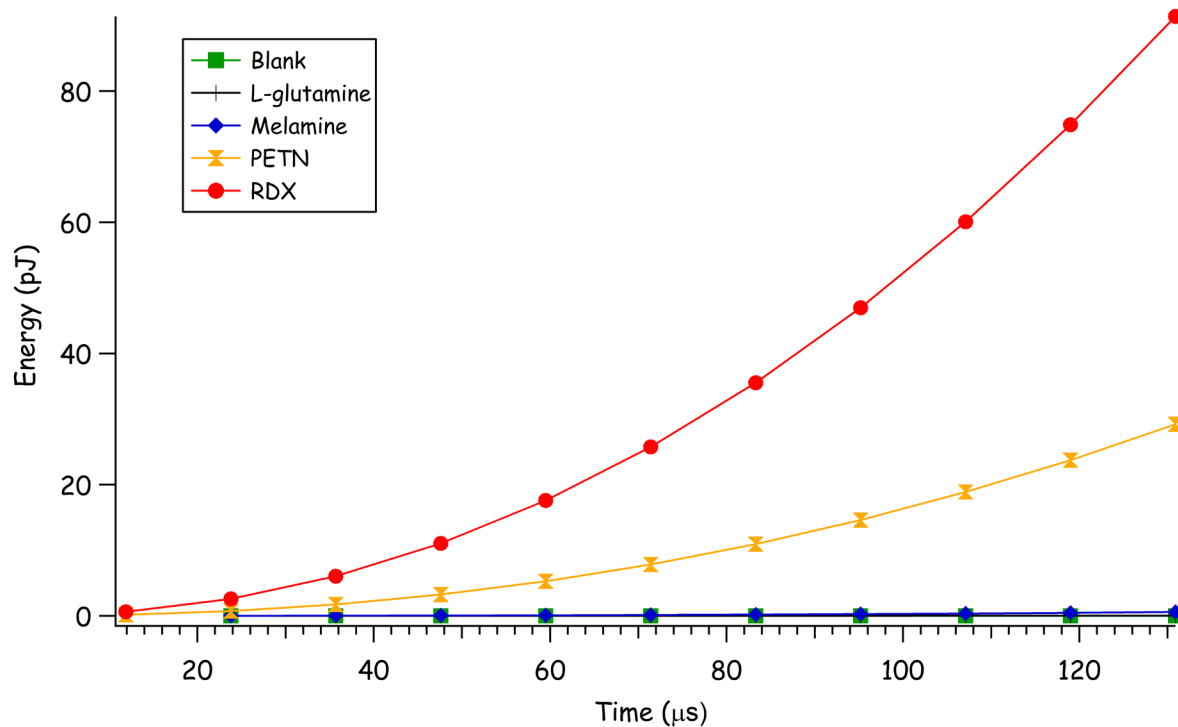
FIG. 12. Calculated time-dependent energy release for energetic and non-energetic samples.

A second model that is often applied to laser-induced shock fronts at longer distances is the drag model (equation 2). Figure 13 shows the fits for the expansion data to the drag model. While the model fits reasonably well to the non-energetic samples, the fit to the energetic samples is extremely poor. The χ^2 values are an order of magnitude higher for the energetic materials (169, 251) than the non-energetic materials (23.5, 10.1, 20.9). The drag model under-predicts the shock velocity for the energetic materials at the times less than 50 µs and greater than 130 µs, further indication that additional energy is put into the plasma by the exothermic reactions.
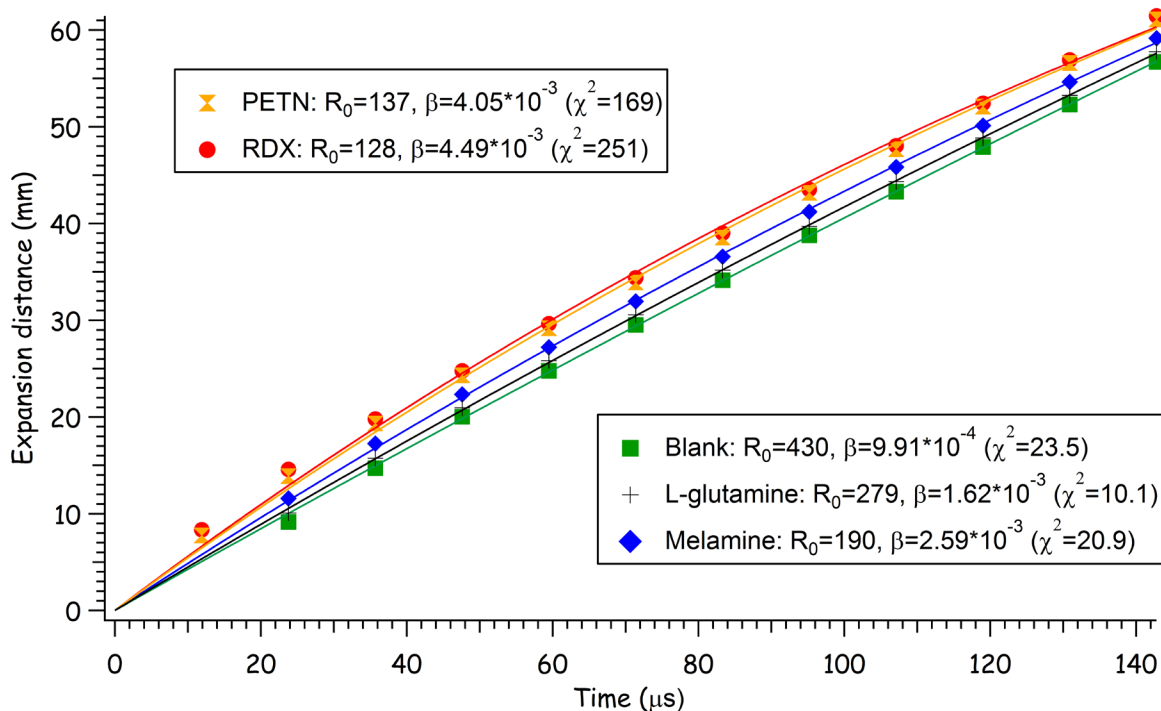
FIG. 13. Expansion distance of the shock waves vs. time demonstrating that the drag model is not valid at these distances.

Dewey[63] fit the shock position versus time for a large-scale TNT detonation (500 tons) to the equation

$$R = A + Bt + C ln(1 + t) + D\left(ln(1 + t)\right)^{1/2}, \tag{10}$$

where A, B, C, and D are fitted coefficients and R and t are the shock radius and time, respectively. As shown in figure 14, the explosive samples RDX and PETN fit very well to equation (10) with $R \approx 0$ at $t = 0$. The fits for the inert materials, on the other hand, predicted a negative shock radius at $t = 0$ (which has no physical meaning). For all samples, $\chi^2 < 1$ indicates that the model is over-fitting the data. Thus, while equation (10) works relatively well for laser-shocked energetic materials, it is not appropriate for the inert materials.
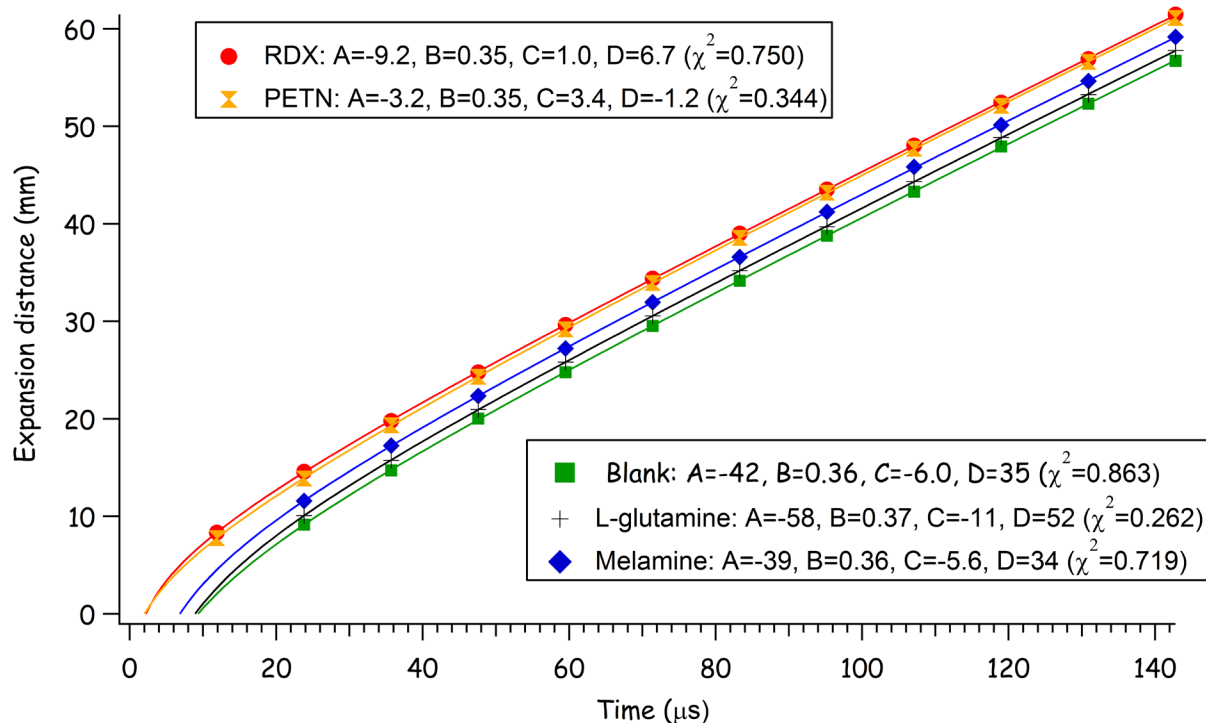
FIG. 14. Expansion distance of the shock waves vs. time fit to the Dewey equation (63).

In order to simplify the data analysis and avoid having to fit the samples to different models depending on whether they were energetic or not, the velocity versus time plot for each sample was fit to a 5th-order polynomial. A 5th-order polynomial was selected to fit the shock data as a compromise between the precision of the measurement (which increased with lower order polynomials) and the quality of the fit (which increased with higher order polynomials). The characteristic air shock velocity for each sample was defined as the y-intercept. The actual velocity of the shock wave at very early times (nanosecond timescale) is on the order of km/s when it is being accelerated by the supersonic expansion of the plasma plume. The y-intercept does not reflect the velocity at time zero, therefore, but the point in time when the shock front expands freely into the ambient air without additional energy input from the laser-induced plasma.

The characteristic air shock velocities for each of the samples were determined; the results are shown in figure 15. The error bars represent 95% confidence intervals and reflect the shot-to-shot variations common with the laser ablation of powdered materials[29,64] and the relatively limited number of laser shots (5) recorded for each non-energetic sample (20-40 laser shots were recorded for each of the energetic samples). The lowest air shock velocities were obtained for the inert materials, including the blank substrate, carbon samples, L-glutamine, and melamine. It has previously been observed that the repulsive force from a hard sample increases the shock wave velocity, while softer samples absorb the recoil energy of the ablated atoms, subsequently decreasing the speed of the shock wave.[65] However, with high laser fluences the recoil force exerted on the surface by the expanding vapor is minimized and the relative hardness of the material is less important.[26] A comparison of the measured air shock velocities for the graphite samples (graphite, GNP, NG) to the diamond shock velocity shows that although the increased hardness of diamond does increase the shock velocity, the addition of energy to the plasma through chemical reactions produces much more significant increases in shock velocity. Nanoparticles such as GNP have a faster rate of energy release than larger micron-size particles such as the graphite and NG,[66] resulting in a higher shock velocity. The standard heat of combustion of sucrose[67] (ΔH_c^0=5644 kJ/mol) is more than twice that of melamine[68] (ΔH_c^0=2455

kJ/mol) and L-glutamine[69] (ΔH_c^0=2572 kJ/mol); the sugar sample produced a higher shock velocity than either the melamine or L-glutamine. While this may indicate some correlation between heat of combustion and shock velocity for the non-energetic materials, the graphite shock velocity is identical to the L-glutamine and melamine, despite having a significantly lower heat of combustion[70] (ΔH_c^0=393.7 kJ/mol). Unlike the other samples, however, the graphite is black and may therefore have directly absorbed more laser energy.
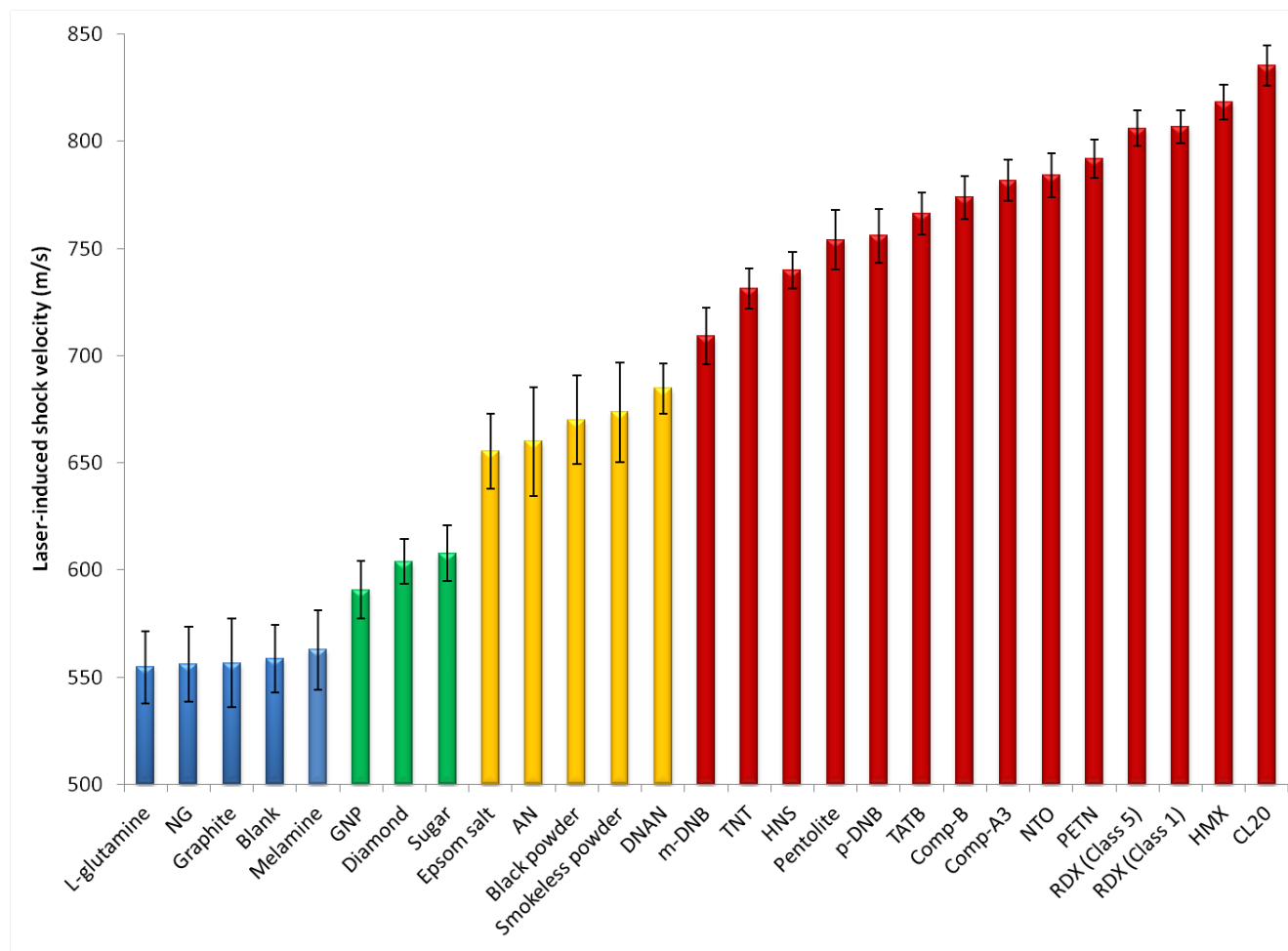
FIG. 15. Characteristic laser-induced shock velocities for non-energetic (<610 m/s) and energetic (>650 m/s) materials. Error bars represent 95% confidence intervals.

Both the Epsom salt and AN produced shock velocities exceeding those of the inert materials. While the low explosives (black powder, smokeless gun powder) also produced larger shock velocities than the inert materials, the high explosives produced the largest air shock velocities of all the materials investigated. The measured laser-induced shock velocities for the energetic materials were strongly correlated to the calculated energies of detonation (r=0.91). DNAN, which has the lowest detonation velocity of the high explosives studied here, produced the lowest laser-induced shock velocity of the high explosive samples. CL-20, the most powerful conventional military explosive, produced the highest shock velocity. These results demonstrate that the laser-induced shock waves can be used to discriminate between energetic and non-energetic materials.

V. CONCLUSIONS

Although previous laser-induced shock studies on metal targets found no evidence for chemical reactions behind the shock front,[4,10] our results indicate that for non-metal samples that undergo exothermic reactions upon decomposition, chemical reactions in the vapor plume behind the shock front affect the shock front velocity. While previous experiments measured the position of the shock wave up to several microseconds using a charge-coupled device camera to capture a single frame from each laser ablation event, this experiment measured the shock wave position up to 200 μs using more than fifteen frames for each event. In addition, the laser pulse energy for this experiment (900 mJ) was considerably higher than typical pulse energies used for laser-induced shock experiments (<200 mJ). Unlike previous laser-induced shock studies on non-energetic materials, the thermal energy in the energetic material vapor plume was caused by both the energy transferred from the laser and the subsequent exothermic chemical reactions of the ablated species. Clear differences in the visible emission, shock structure, and heat-affected zones were observed between the inert and energetic materials. The Sedov-Taylor model was not applicable for any of the samples studied here because of the distance from the target and because of the chemical reactions in the plasma. While the drag model worked well for inert materials, the Dewey fit worked best for the energetic materials. No single model could be found to fit both energetic and non-energetic materials. Based on the initial promising results that demonstrate a correlation between the laser-induced shock velocity and explosive performance, a new laboratory-scale method for predicting detonation velocities and pressures using milligram quantities of material is currently being developed in our laboratory. Those results will be presented in a forthcoming paper.

ACKNOWLEDGMENTS

REFERENCES

[1] F. Brech and L. Cross, "Optical microemission stimulated by a ruby laser," Appl. Spectrosc. **16,** 59 (1962).

[2] R. B. Hall, "Laser Production of Blast Waves in Low Pressure Gases," J. Appl. Phys. **40,** 1941 (1969).

[3] J. Grun, J. Stamper, C. Manka, J. Resnick, R. Burris, and B. H. Ripin, "Observation of high-pressure blast-wave decursors," Appl. Phys. Lett. **59,** 246 (1991).

[4] G. Callies, P. Berger, and H. Hugel, "Time-resolved observation of gas-dynamic discontinuities arising during excimer laser ablation and their interpretation," J. Phys. D **28,** 794 (1995).

[5] X. Zeng, X. L. Mao, R. Greif, and R. E. Russo, "Experimental investigation of ablation efficiency and plasma expansion during femtosecond and nanosecond laser ablation of silicon," Appl. Phys. A **80,** 237 (2005).

[6] S.-B. Wen, X. Mao, R. Greif, and R. E. Russo, "Expansion of the laser ablation vapor plume into a background gas. I. Analysis," J. Appl. Phys. **101,** 023114 (2007).

[7] S.-B. Wen, X. Mao, R. Greif, and R. E. Russo, "Laser ablation induced vapor plume expansion into a background gas. II. Experimental analysis," J. Appl. Phys. **101,** 023115 (2007).

[8] Z.-y. Zheng, Y. Zhang, C.-c. Zhao, H.-y. Hao, X. Lu, Y.-t. Li, and J. Zhang, "Ablation pressure of the shock wave generated by laser interaction with solid targets," Optelec. Lett. **3,** 394 (2007).

9   S. Amoruso, J. Schou, and J. Lunney, "Influence of the atomic mass of the background gas on laser ablation plume propagation," Appl. Phys. A 92, 907 (2008).

10 J. J. Yoh, H. Lee, J. Choi, K.-c. Lee, and K.-h. Kim, "Ablation-induced explosion of metal using a high-power Nd:YAG laser," J. Appl. Phys. 103, 043511 (2008).

11 J.-F. Y. Gravel and D. Boudreau, "Study by focused shadowgraphy of the effect of laser irradiance on laser-induced plasma formation and ablation rate in various gases," Spectrochim. Acta, Part B 64, 56 (2009).

12 C. Porneala and D. A. Willis, "Time-resolved dynamics of nanosecond laser-induced phase explosion," J. Phys. D-Appl. Phys. 42, 155503 (2009).

13 S. S. Harilal, G. V. Miloshevsky, P. K. Diwakar, N. L. LaHaye, and A. Hassanein, "Experimental and computational study of complex shockwave dynamics in laser ablation plumes in argon atmosphere," Phys. Plasmas 19, 083504 (2012).

14 M. Thiyagarajan, K. Williamson, and A. R. Kandi, "Experimental Investigation of 1064-nm IR Laser-Induced Air Plasma Using Optical Laser Shadowgraphy Diagnostics," IEEE Trans. Plasma Sci. 40, 2491 (2012).

15 R. Sanginés and H. Sobral, "Time resolved study of the emission enhancement mechanisms in orthogonal double-pulse laser-induced breakdown spectroscopy," Spectrochim. Acta, Part B 88, 150 (2013).

16 Y. Ben-Eliahu, Y. Haas, and S. Welner, "Laser Initiation of the Decomposition of Energetic Polymers: Shock Wave Formation," J. Phys. Chem. 99, 6010 (1995).

17 Y. Haas, Y. Ben-Eliahu, and S. Welner, "Pulsed Laser Induced Decomposition of Energetic Polymers: Comparison of ultraviolet (355 nm) and infrared (9.3 μm) initiation," Propellants, Explos., Pyrotech. 21, 258 (1996).

18 L. Belau, Y. Ben-Eliahu, I. Hecht, G. Kop, Y. Haas, and S. Welner, "Laser-Induced Dissociation of an Energetic Polymer: A Spectroscopic Study of the Gaseous Products," J. Phys. Chem. B 104, 10154 (2000).

19 M. Hauer, D. J. Funk, T. Lippert, and A. Wokaun, "Time resolved study of the laser ablation induced shockwave," Thin Solid Films 453-454, 584 (2004).

20 S. Roy, N. Jiang, H. U. Stauffer, J. B. Schmidt, W. D. Kulatilaka, T. R. Meyer, C. E. Bunker, and J. R. Gord, "Spatially and temporally resolved temperature and shock-speed measurements behind a laser-induced blast wave of energetic nanoparticles," J. Appl. Phys. 113, 184310 (2013).

21 F. C. De Lucia Jr. and J. L. Gottfried, "Characterization of a series of nitrogen-rich molecules using laser-induced breakdown spectroscopy," Propellants, Explos., Pyrotech. 35, 268 (2010).

22 J. L. Gottfried, "Laser-induced plasma chemistry of the explosive RDX with various metallic nanoparticles," Appl. Opt. 51, B13 (2012).

23 J. L. Gottfried and J. M. Densmore, "Laser-Induced Breakdown Spectroscopy of Reactive Materials Doped with Carbon Nanoparticles," JANNAF J. Prop. Energ. 6, 23 (2013).

24 F. C. De Lucia and J. L. Gottfried, "Influence of Molecular Structure on the Laser-Induced Plasma Emission of the Explosive RDX and Organic Polymers," J. Phys. Chem. A 117, 9555 (2013).

25 A. Bogaerts, Z. Chen, R. Gijbels, and A. Vertes, "Laser ablation for analytical sampling: what can we learn from modeling?," Spectrochim. Acta, Part B 58, 1867 (2003).

26 M. von Allmen and A. Blatter, *Laser-Beam Interactions with Materials: Physical Principles and Applications*, 2nd ed. (Springer-Verlag, Berlin Heidelberg, 2002).

27 S. S. Harilal, C. V. Bindhu, M. S. Tillack, F. Najmabadi, and A. C. Gaeris, "Internal structure and expansion dynamics of laser ablation plumes into ambient gases," J. Appl. Phys. 93, 2380 (2003).

28   D. A. Cremers and L. J. Radziemski, *Handbook of Laser-Induced Breakdown Spectroscopy*, 2nd ed. (John Wiley & Sons, Ltd., Singapore, 2013).

29   J. L. Gottfried, F. C. De Lucia Jr, C. A. Munson, and A. W. Miziolek, "Laser-induced breakdown spectroscopy for detection of explosives residues: a review of recent advances, challenges, and future prospects," Anal. Bioanal. Chem. 395, 283 (2009).

30   F. C. De Lucia Jr. and J. L. Gottfried, "Classification of explosive residues on organic substrates using laser induced breakdown spectroscopy " Appl. Opt. 51, B83 (2012).

31   P. Lucena, I. Gaona, J. Moros, and J. J. Laserna, "Location and detection of explosive-contaminated human fingerprints on distant targets using standoff laser-induced breakdown spectroscopy," Spectrochim. Acta, Part B 85, 71 (2013).

32   R. Singh, "Transient plasma shielding effects during pulsed laser ablation of materials," J. Electron. Mater. 25, 125 (1996).

33   R.G. Root, "Modeling of post-breakdown phenomena" in *Laser-induced plasma and applications*, L. J. Radziemski and D. A. Cremers, ed. (Marcel Dekker, New York, 1989).

34   G. Taylor, "The formation of a blast wave by a very intense explosion I. Theoretical discussion," Proc. R. Soc. A 201, 159 (1950).

35   M. Aden, E. W. Kreutz, H. Schlüter, and K. Wissenbach, "The applicability of the Sedov - Taylor scaling during material removal of metals and oxide layers with pulsed CO_2 and excimer laser radiation," J. Appl. Phys. D 30, 980 (1997).

36   L. I. Sedov, *Similarity and Dimensional Methods in Mechanics* (Cleaver Hume, London, 1959).

37   W. E. Maher and R. B. Hall, "An interferometric investigation of laser - supported absorption waves," J. Appl. Phys. 46, 761 (1975).

38   S. A. Ramsden and P. Savic, "A Radiative Detonation Model for the Development of a Laser-Induced Spark in Air," Nature 203, 1217 (1964).

39   Y. P. Raizer, "Heating of a gas by a powerful light pulse," Sov. Phys.-JETP 21, 1009 (1965).

40   W. E. Maher, R. B. Hall, and R. R. Johnson, "Experimental study of igition and propagation of laser-supported detonation waves," J. Appl. Phys. 45, 2138 (1974).

41   M. Ushio, K. Komurasaki, K. Kawamura, and Y. Arakawa, "Effect of laser supported detonation wave confinement on termination conditions," Shock Waves 18, 35 (2008).

42   C.-h. Kim, G. B. Ardian, and J. J. Yoh, "Surface chemical reaction of laser ablated aluminum sample for detonation initiation," J. Appl. Phys. 109 (2011).

43   D. B. Geohegan, "Fast intensified-CCD photography of $YBa_2Cu_3O_{7-x}$ laser ablation in vacuum and ambient oxygen," Appl. Phys. Lett. 60, 2732 (1992).

44   A. Kushwaha and R. K. Thareja, "Dynamics of laser-ablated carbon plasma: formation of C_2 and CN," Appl. Opt. 47, G65 (2008).

45   J. Gonzalo, C. N. Afonso, and I. Madariaga, "Expansion dynamics of the plasma produced by laser ablation of $BaTiO_3$ in a gas environment," J. Appl. Phys. 81, 951 (1997).

46   P. E. Dyer and J. Sidhu, "Spectroscopic and fast photographic studies of excimer laser polymer ablation," J. Appl. Phys. 64, 4657 (1988).

47   F. Kokai, K. Takahashi, K. Shimizu, M. Yudasaka, and S. Iijima, "Shadowgraphic and emission imaging spectroscopic studies of the laser ablation of graphite in an Ar gas atmosphere," Appl Phys A 69, S223 (1999).

48   A. Salleo, F. Y. Genin, M. D. Feit, A. M. Rubenchik, T. Sands, S. S. Mao, and R. E. Russo, "Energy deposition at front and rear surfaces during picosecond laser interaction with fused silica," Appl. Phys. Lett. 78, 2840 (2001).

49   X. Zeng, X. Mao, S.-B. Wen, R. Greif, and R. E. Russo, "Energy deposition and shock wave propagation during pulsed laser ablation in fused silica cavities," J. Phys. D 37, 1132 (2004).

50 N. Zhang, X. Zhu, J. Yang, X. Wang, and M. Wang, "Time-Resolved Shadowgraphs of Material Ejection in Intense Femtosecond Laser Ablation of Aluminum," Phys. Rev. Lett. 99, 167602 (2007).

51 T. A. Schmitz, J. Koch, D. Günther, and R. Zenobi, "Early plume and shock wave dynamics in atmospheric-pressure ultraviolet-laser ablation of different matrix-assisted laser ablation matrices," J. Appl. Phys. 109 (2011).

52 G. S. Settles, *Schlieren and Shadowgraph Techniques* (Springer-Verlag, New York, 2001).

53 T. Shimizu, in *Proceedings of the 15th International Pyrotechnics Seminar,* "*An example of negative explosives: magnesium sulfate/magnesium mixture*", Boulder, CO, 1990 (Journal of Pyrotechnics Inc.).

54 A. E. Kramida, Y. Ralchenko, J. Reader, and N. A. Team (2013). *NIST Atomic Spectra Database (version 5.1)*, [Online]. Available: http://physics.nist.gov/asd [5 Jun 2014]. National Institute of Standards and Technology, Gaithersburg, MD.

55 V. P. Sinditskii, V. Y. Egorshev, A. I. Levshenkov, and V. V. Serushkin, "Ammonium Nitrate: Combustion Mechanism and the Role of Additives," Propellants, Explos., Pyrotech. 30, 269 (2005).

56 H. L. Brode, "The Blast Wave in Air Resulting From a High Temperature, High Pressure Sphere of Air," Report No. RM-1825-AEC (US Atomic Energy Commission, Santa Monica, CA, 1956).

57 D. A. Freiwald and R. A. Axford, "Approximate spherical blast theory including source mass," J. Appl. Phys. 46, 1171 (1975).

58 S. H. Jeong, R. Greif, and R. E. Russo, "Propagation of the shock wave generated from excimer laser heating of aluminum targets in comparison with ideal blast wave theory," Appl. Surf. Sci. 127–129, 1029 (1998).

59 S. H. Jeong, R. Greif, and R. E. Russo, "Shock wave and material vapour plume propagation during excimer laser ablation of aluminium samples," J. Phys. D 32, 2578 (1999).

60 L. S. Bennett, T. Lippert, H. Furutani, H. Fukumura, and H. Masuhara, "Laser induced microexplosions of a photosensitive polymer," Appl. Phys. A 63, 327 (1996).

61 R. Srinivasan, B. Braren, K. G. Casey, and M. Yeh, "Ultrafast imaging of ultraviolet laser ablation and etching of polymethylmethacrylate," Appl. Phys. Lett. 55, 2790 (1989).

62 G. J. Hutchens, "Approximate near-field blast theory: A generalized approach," J. Appl. Phys. 88, 3654 (2000).

63 J. M. Dewey, "The Properties of a Blast Wave Obtained from an Analysis of the Particle Trajectories," Proc. Roy. Soc. A 324, 275 (1971).

64 J. L. Gottfried, F. C. De Lucia Jr, C. A. Munson, and A. W. Miziolek, "Standoff Detection of Chemical and Biological Threats Using Laser-Induced Breakdown Spectroscopy," Appl. Spectrosc. 62, 353 (2008).

65 K. Tsuyuki, S. Miura, N. Idris, K. H. Kurniawan, T. J. Lie, and K. Kagawa, "Measurement of Concrete Strength Using the Emission Intensity Ratio Between Ca(II) 396.8 nm and Ca(I) 422.6 nm in a Nd:YAG Laser-Induced Plasma," Appl. Spectrosc. 60, 61 (2006).

66 D. D. Dlott, "Thinking big (and small) about energetic materials," Mater. Sci. Technol. 22, 463 (2006).

67 P. Cooper, *Explosives Engineering* (Wiley-VCH, New York, 1996).

68 P. Liu, W. Xiong, S.-Z. Hu, X. Li, and Z.-C. Tan, "Enthalpy of Formation, Heat Capacity and Entropy of Melamine," Acta Physico-Chimica Sinica 25, 2417 (2009).

69 J. D. Cox and G. Pilcher, *Thermochemistry of Organic and Organometallic Compounds* (Academic Press, New York, 1970).

70 P. Hawtin, J. B. Lewis, N. Moul, and R. H. Phillips, "The Heats of Combustion of Graphite, Diamond and Some Non-Graphitic Carbons," Phil. Trans. R. Soc. Lond. A 261, 67 (1966).